

## Influence of AC Stray Current on Cathodic Disbondment of Epoxy Coatings

Qingmiao Ding<sup>1</sup>, Zili Li<sup>2</sup>, Dilinuer Dilimulati<sup>1</sup>, Deyou Wang<sup>1</sup>, Xiaoyu Shi<sup>1</sup>

<sup>1</sup> Airport College, Civil Aviation University of China, Tianjin, P. R. China

<sup>2</sup> College of Pipeline and Civil Engineering, China University of Petroleum, Qingdao, P. R. China

Correspondence: Qingmiao Ding, Airport College, Civil Aviation University of China, Tianjin, 300300, P. R. China. Tel: 15122831876.

\*E-mail: [qmding@cauc.edu.cn](mailto:qmding@cauc.edu.cn)

Received: 18 October 2018 / Accepted: 14 March 2020 / Published: 30 November 2020

---

In this paper, the influence of alternating stray current (AC) on the anti-cathode disbonding performance of FBE anti-corrosion layers was studied by an electrochemical method using a high temperature simulation experiment. The results show that the AC stray current promotes the cathodic disbondment of the epoxy powder coating. Because the existence of AC stray currents could increase the replacement rate of the hydrogen evolution reaction and the anodic corrosion on the coating disbonding, the interference of the AC stray current exacerbates the degree of anode corrosion, which indirectly leads to a shorter cycle of the anode-anode reaction. Thus, the disbonding speed is increased, and the degree of cathodic disbonding of the epoxy powder coating increases as the applied AC stray current increases.

---

**Keywords:** Epoxy powder coating, AC stray current, cathodic disbonding, disbonding speed, disbonding degree

### 1. INTRODUCTION

Today's buried oil and gas pipelines mostly use anti-corrosion coatings and cathodic protection to form the external corrosion control system of the pipeline [1]. In the selection of the anti-corrosion layer, a fusion-bonded epoxy (FBE) powder anti-corrosion layer is used [2,3], which has excellent anti-corrosion performance, strong pipe adhesion and good compatibility with the protected system. Currently, it is the most widely used and most recognized pipeline anti-corrosion layer, but at the same time it is also sensitive to impact collision and poor waterproof performance [4, 5], so the FBE anti-corrosion coating will inevitably appear to be damaged and aged during long-term service of the pipeline [6-8]. In practical engineering applications, the method of increasing the cathodic protection

output potential is usually adopted to ensure the anti-corrosion effect of the pipeline. However, the high potential is likely to cause the metal potential of some defects to be excessively negative and result in electron accumulation. Excess hydroxide ions are formed at the defect sites because of oxygen, water and hydrogen ions generated after water ionization; that is, the pipeline is overprotected. Excess  $\text{OH}^-$  is formed in the cathode region, which forms an alkaline environment, reduces the adhesion of the coating and the metal, and causes the disbonding phenomenon of the coating layer, namely, cathodic disbonding [9-12].

There are many research studies on the cathodic stripping of organic coatings; however, few investigators have attempted to understand its mechanism [14-17]. The peeling resistance of the organic coating is an important parameter for determining whether the coating is qualified [13]. In the case of rubber/metal composites, Stevenson discovered that a rapid adhesion failure occurred when cathodic polarization was applied when testing samples in seawater. Cathodic delamination of organic coating is mainly affected by design parameters of coating, physical and testing parameters [1]. The physical and testing parameters include thickness of the coating, testing temperature, electrolyte composition, dissolved oxygen, surface roughness and cathodic potential. Khun and Frankel [18] found that the cathodic delamination rate of epoxy coatings dramatically decreased with increased surface roughness of the underlying steel substrate. Similarly, the effect of coating thickness [1, 19–22], applied cathodic potential [19,21,23,25] and testing temperature [22,24,25] on cathodic delamination resistance were also studied by some researchers. The general trend [26-32] found in these studies is that rate of coating delamination increases with decreasing coating thickness, application of more negative cathodic potentials and increasing temperature.

Most of these studies used lower temperatures and less negative cathodic potentials than those suggested in standard test methods. In addition, research on the effect of stray current on the anti-cathode disbonding performance of epoxy powder coating without defects is relatively sparse [33]. Therefore, the effect of AC stray current on the cathodic disbonding performance of single-layer fusion bonded epoxy powder coating is studied and reported here. We employed different AC stray currents, and we measured and analyzed the cathodic protection current and electrochemical impedance spectrum at different time points during the test. These were combined with the disbonding radius of the coating and the topography of the stripped metal surface and comprehensively analyzed. Thus, we obtained the influence of the scattered current on the anti-cathode stripping performance of the anti-corrosion layer.

## **2. EXPERIMENT**

### *2.1. Experimental sample*

The test piece used for the test was a section of a Q235 steel pipe coated with a sintered epoxy powder coating having a coating thickness of 400  $\mu\text{m}$  and a slice size of 150 mm $\times$ 150 mm  $\times$ 10 mm. The slice was tested with a spark leak detector; the leak detection voltage was set to 2000 V. Eligible

test strips were selected for the experiment, and each set of experiments was performed using three parallel samples for simultaneous testing.

## 2.2. Experimental methods

The experimental setup is shown in Figure 1. A first blind hole with a diameter of 3.2 mm was made at the center of the test sample to expose the metal substrate. A first PVC tube with a diameter of 75 mm and a height of 12 cm was selected, and the center of the tube was aligned with the center of the first blind hole at the center of the sample. The first tube formed an edge seal with the first blind hole that prevented water leakage. In a 10 mm × 10 mm region at the corner of the sample, a second blind hole with a diameter of 3.2 mm was formed in the center of the area. A second PVC tube with a diameter of 25 mm and a height of 12 cm was selected. The center of the second PVC pipe was aligned with the center of the second blind hole at the corner of the sample. The second tube formed an edge seal with the second blind hole that prevented water leakage. A platinum electrode was used as an auxiliary electrode for applying stray current, and an AC power supply provided AC stray current interference for the experimental system. The corner opposite the corner with the second blind hole of the experimental sample was polished to remove the coating, and a platinum electrode was selected as the auxiliary anode. The sample and the auxiliary anode were connected to the DC stabilized power source to provide cathodic protection for the experimental system and to control the cathodic protection potential of -3.5 V. A 3.5% NaCl solution heated to 65°C was poured into the two PVC tubes, and the experimental temperature was controlled at 65°C. During the experiment, the liquid level was maintained at 3/4 of the tube height. The entire experiment took 48 hours.

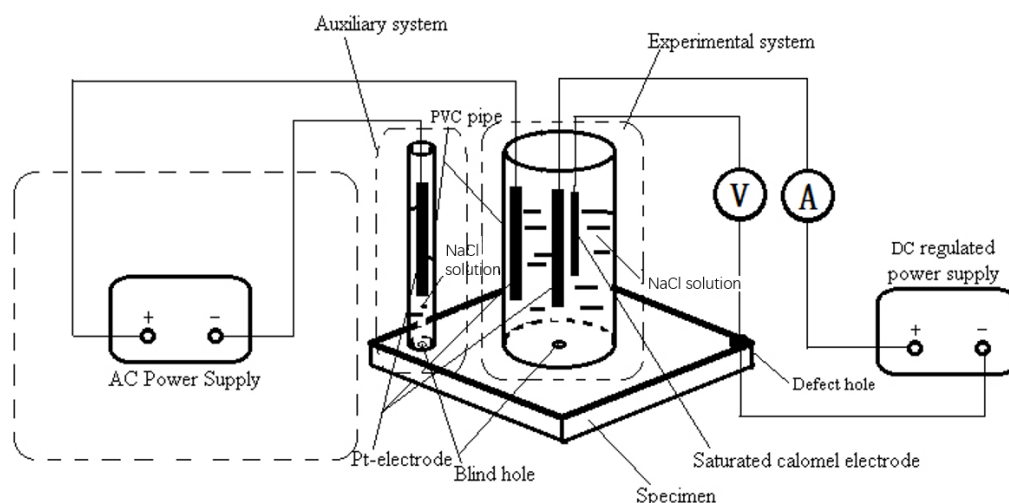


**Figure 1.** The experimental device diagram

## 2.3 Experimental program

After the experimental device was built, the appropriate potential was applied to bring the cathodic protection potential to -3.5 V. The AC interference voltages applied to the test specimens

were 4 V, 6 V, 8 V and 16 V, respectively. The entire experiment took 48 hours, and the current value was measured and recorded when the test sample was immersed for 0 h, 7 h, 20 h, 27 h, 34 h, 44 h, and 48 h.

### 2.3.1 Electrochemical test

Electrochemical experiments were performed with the electrochemical workstation. The connection mode is shown in Figure 2. A three-electrode system was used. The working electrode was a coated metal system, the auxiliary electrode was a platinum electrode, and the reference electrode was a saturated calomel electrode. The electrochemical impedance spectroscopy test frequency ranged from 0.1 Hz to 100 kHz, and the amplitude was 10 mV. Electrochemical impedance spectroscopy data were fitted with ZsimpWin software.

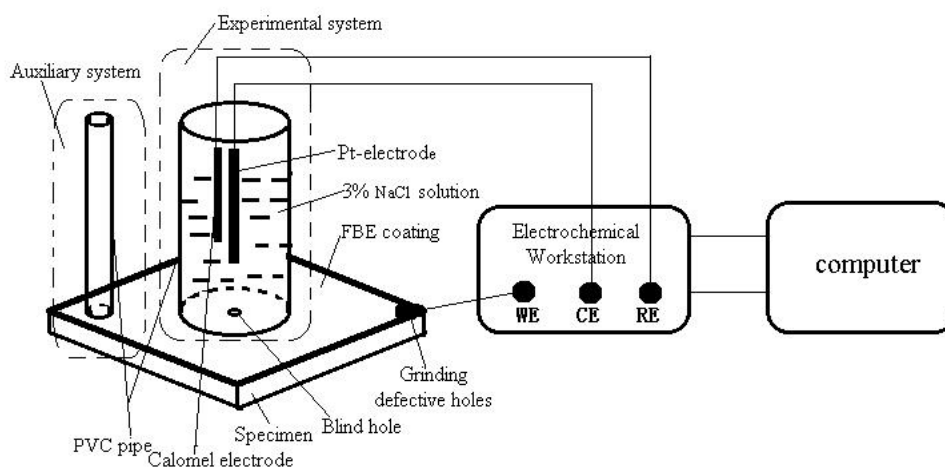


**Figure 2.** Schematic diagram of electrochemical impedance testing device

### 2.3.2 The cathodic disbonding test

After the end of the experiment, the samples were taken out, cooled to room temperature, and subjected to the cathodic peel test within 1 hour after the power was turned off. As shown in Figure 3, the coating was cut through to expose the metal substrate by using a knife. The knife was then inserted along the underside of the coating from the test hole and the coating was peeled along the scribe lines with a horizontal force until the coating exhibited significant resistance to disbonding. The disbonding distance of each scribe line was measured from the edge of the blind hole, and the average value was obtained, which was the cathode disbonding distance of the test piece. The arithmetic mean of the cathodic disbonding distances of the three parallel experimental specimens was expressed to the nearest 0.1 mm. The three test parameters of cathodic protection current, electrochemical impedance and cathodic disbondment distance were selected to summarize the influence law.

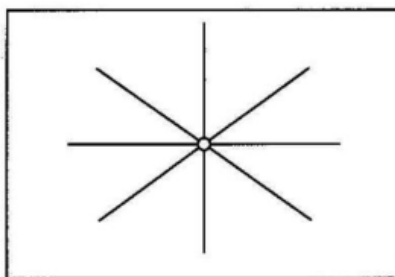


**Figure 3.** The cathodic peel test diagram

### 2.3.3 Morphology analysis

The peeled test pieces after the experiment were naturally dried on the test bench. When they were cooled to room temperature, the corrosion morphology was observed by scanning electron microscopy (SEM), and the elemental composition of the surface corrosion product was analyzed by energy spectrum.

## 3. RESULTS AND DISCUSSION

### 3.1 Effect on cathodic protection current

The cathodic protection current obtained by applying different sizes of AC stray currents is shown in Figure 4.

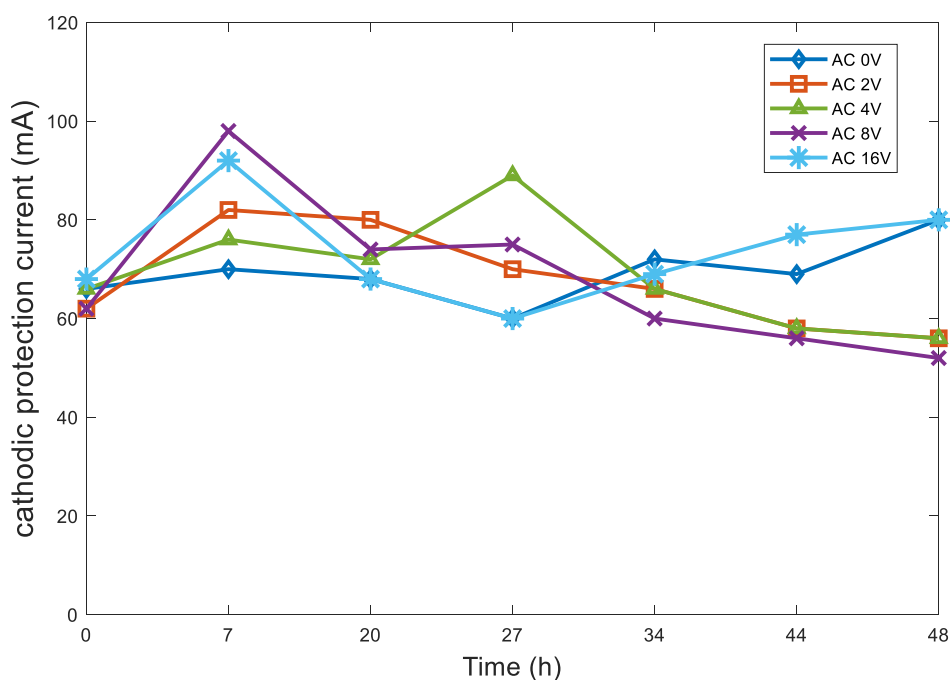


**Figure 4.** The cathodic protection current under 0 V, 2 V, 4 V, 8 V and 16 V AC interference

Each test cathodic protection current line in Figure 4 fluctuates with time, and the greater the intensity of the applied AC interference, the more severe the fluctuation. The cathodic protection current of each test group with AC interference increased greatly at 7 h, although the changes of the blank group without AC interference are not very evident. The cathodic protection current of the blank test group and the test group with AC interference of 16 V fluctuated after 27 h, while the current values of other test groups with AC interference showed a fluctuating downward trend. The test groups with AC interference of 2 V, 8 V and 16 V reached the maximum values in the test period at 7 h, while the test group with AC interference of 4 V and blank test group showed maximum values at 27 h and 48 h, respectively.

When the tube sample is cathodically protected, the applied cathodic protection current is  $|I_-|$ . According to the current summation principle [34], the formula of the cathodic protection current can be written:

$$\begin{aligned} I_3 &= |I_1| - I_2 \\ |I_-| &= |I_0| + I_3 \end{aligned} \quad (1)$$

where  $|I_0|$  represents the cathodic protection current at the beginning of the test,  $|I_1|$  represents the change in the cathode reaction current of the metal electrode,  $I_2$  represents the anode current produced by the metal electrode, and  $I_3$  represents the changed value of the cathodic protection current during the experiment.

Because  $|I_1|$  and  $I_2$  are both dominant, the positive and negative changes of  $I_3$  are revealed – that is, the fluctuations reflected in Figure 4. In the test, as the degree of disbonding of the coating increases, the exposed metal area under the coating increases, which results in an asymmetrical cathodic protection potential, and the cathodic protection current shielding occurs [33], which results in an increase in anodic corrosion; that is,  $I_2$  increases. This is reflected in the value of  $I_3$ , which first increases and then decreases, as seen in the fluctuation of the cathodic protection current.

When the test was carried out for 7 hours, the coating of the test group had been significantly peeled off, and the area of the coating defect increased; the degree of disbonding of the blank group without AC interference was significantly smaller than the other groups with AC interference.

Within 27 hours after the experiment started, the cathode reaction current of the blank group without AC interference had a small fluctuation. This fluctuation indicates that the disbonding degree of the test specimen was still small. After 27 hours, the current fluctuation increased. This increase indicates that the cathode disbonding dominated and the disbonding of the coating was intensified. After a 7 h-27 h current drop, the current of the test group with AC interference of 16 V began to increase again. The reason may be that the alternating cycle between the cathodic reaction and the anodic corrosion becomes shorter, and the corrosion reaction rate is significantly accelerated [35].

The cathode reaction caused the coating to peel off before 7 h, so the closed loop resistance value was significantly reduced, and the electron transfer rate was accelerated. Therefore, the cathodic protection current values with AC interferences of 2 V, 8 V and 16 V reached the maximum value at 7 h. The decrease of the current after 7 h indicates that the effect of AC stray current on metal corrosion is more and more evident with time, which leads to the increase of corrosion reaction and the resistance increase that hinders the current is greater than the resistance reduction value of the coating

failure [36]. The maximum cathodic protection current value with AC interference of 4 V occurred at 27 h. This may be due to uneven filler and thickness of the coating.

### 3.2 Influence on electrochemical impedance of the system

For the impedance spectrum obtained by the experiments, a large number of equivalent circuit models were used to fit them. In the experiment with AC interference of 2 V, the best equivalent circuit model selected for soaking for 7 h and 20 h is C(R(RC)), as shown in Figure 5, the best circuit for immersion for 27 h is C(R(RW)), as shown in Figure 6, and the best circuit for immersion for 34 h, 44 h and 48 h is R(C(RW)), as shown in Figure 7. The impedance values of the components of the analog circuit with AC interference of 2 V are shown in Table 1.

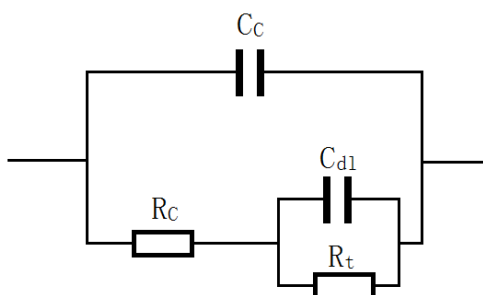


**Figure 5.** Equivalent circuit model C(R(RC))

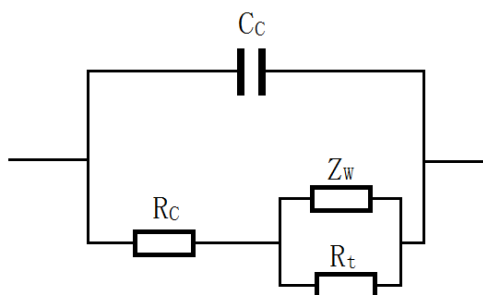


**Figure 6.** Equivalent circuit model C(R(RW))

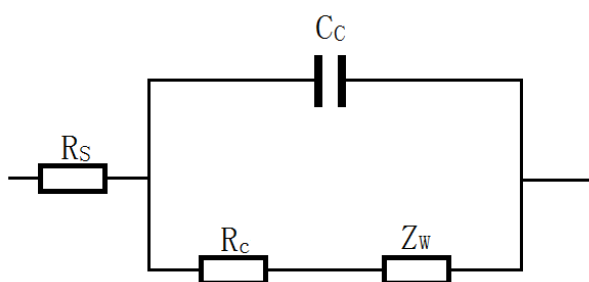


**Figure 7.** Equivalent circuit model RC(RW)

**Table 1.** The impedance values of the components of the analog circuit with AC interference of 2 V

	7 h	20 h	27 h	34 h	44 h	48 h
$R_s$	/	/	/	0.1582	0.1897	0.195
$C_c$	1.034E-7	1.014E-7	9.727E-8	5.048E-5	4.967E-5	5.365E-5
$R_c$	2.392	1.84	2.339	2.399	2.996	3.083
$C_{dl}$	0.00027	0.7785	/	/	/	/
$R_t$	0.3007	0.3061	4.222	/	/	/
$W$	/	/	0.239	0.01386	4.144	2.042

where  $R_s$  is the resistance of the solution,  $C_c$  is the coating capacitance,  $R_c$  is the combined resistance of the corrosion product of the coating and the metal surface,  $C_{dl}$  is the electric double layer capacitance,  $R_t$  is the charge transfer resistance, and  $Z_w$  is the Warburg impedance. The Warburg impedance is decomposable and becomes a parallel form of two components of diffusion impedance and diffusion capacitance [37].

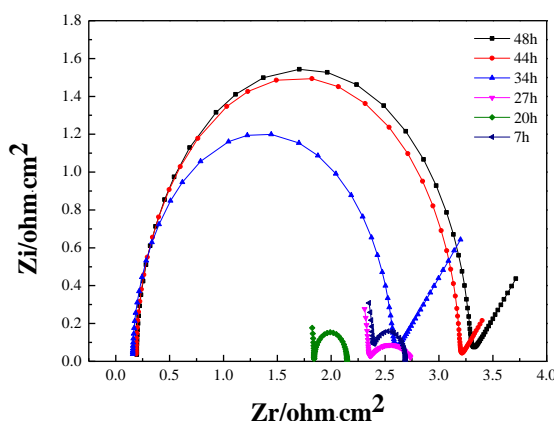


**Figure 8.** Nyquist diagrams of the experiment with AC interference of 2 V

The evolution of the impedance spectrum with time under the 2 V AC interference is shown in Figure 8. From 7 h to 20 h, the arc radius of the high frequency band is reduced, and the arc of the low frequency band is slightly larger. At 20 h, the electrochemical impedance curve intersects the X axis, and it can be seen in the Table 1 that the  $R_c$  value is reduced somewhat, which indicates that the resistance reduction caused by the disbonding of the coating is greater than the increase of the resistance due to corrosion. That is, the coating has been disbonding off at 20 h, and the degree of disbonding is large with respect to 7 h. At 27 h,  $W$  impedance appears, which indicates a new change in the relationship between the coating and the metal surface. In Figure 8, the arc radius of the high and low frequency band increases with respect to 20 h, while the arc is somewhat deformed because of the  $W$  impedance [37]. The  $R_c$  value becomes larger again at 27 h, and the reason may be that the corrosion product on the surface of the coating increases, and the integrated value of the coating and

the corrosion product (that is, the  $R_c$  value) increases. The  $R_t$  value suddenly increases at 27 h, indicating that the coating disbonding progresses to a new stage. Because the disbonding area increases, the coating filler encountered during the media transformation in the tangential direction increases; that is, the resistance to the dielectric charge transfer increases and results in a superposition effect, and the appearance of the  $W$  value confirms this phenomenon [19]. From 34 h to 48 h, as shown in Figure 8, a 45-degree fold line with significant Warburg impedance characteristics appears. This means that the coating has substantially lost its ability to prevent solution intrusion. At this time, the porosity of the coating and the foaming zone of the coating and the metal interface are both large, and the degree of disbonding of the coating greatly increases. The complete arc appears in the high frequency band. Combined with Table 1, the appearance of  $R_s$  also indicates that the coating impedance at this time is greatly reduced, and results in an increase in the specific resistance of the solution in the whole system, which cannot be ignored. From 34 h to 48 h, the  $C_c$  value increases by a magnitude relative to the previous value which indicates that the disbonding area of the coating and the corresponding metal area are increasing. For the  $R_c$  value, the corrosion degree also greatly increases, and the  $R_c$  value increases as a result. The impedance value increases first and then rises from 27 h to 48 h, which means that the coating has a transitional stripping from 27 h to 34 h, which results in a superposition effect of the medium conduction obstruction at 44 h, and the impedance is further reduced at 48 h. The reduction indicates that a small degree of cathodic dissection is still being carried out within 34 h-48 h, and it can be speculated that this stage is the incubation period of a new stage of large-scale exfoliation [19].

In the test with AC interference of 4 V, the best circuit model at the 7 h and 20 h is  $C(R(RC))$ , and the best circuit model is  $C(R(RW))$  after 27 h. The impedance value of the components of the analog circuit is shown in Table 2.

**Table 2.** The impedance value of the components of the analog circuit of the test with AC interference of 4 V

	7 h	20 h	27 h	34 h	44 h	48 h
$R_s$	/	/	/	/	/	/
$C_c$	1.068E-7	4.913E-8	4.203E-8	6.172E-8	6.275E-8	5.636E-8
$R_c$	1.596	2.776	1.917	2.685	3.267	2.777
$C_{dl}$	0.02211	0.1817	/	/	/	/
$R_t$	0.1858	2.908	4.042	0.7409	1.717	1.346
$W$	/	/	0.2215	0.1728	0.2393	0.1867

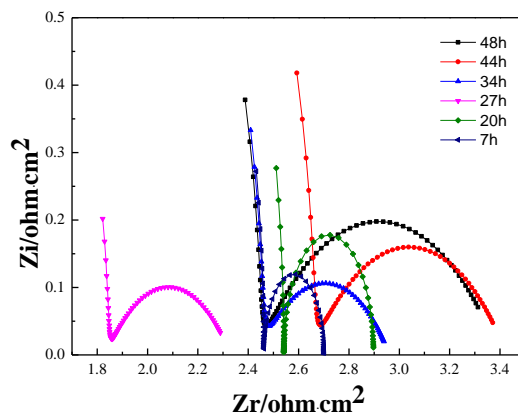


**Figure 9.** Nyquist diagrams of the test with AC interference of 4 V

The evolution of the impedance spectrum over time in the test system with 4 V AC interference is shown in Figure 9. Compared with the spectrum of 2 V AC interference, the range of impedance values is reduced overall. This indicates that the impedance characteristics of the coating are reduced. The 4 V AC interference further promotes stripping of the coating. Moreover, it can be seen from Figure 9 that the radius of the middle and low frequency arc is large and small, respectively, and the main parameters reflecting the arc are  $C_{dl}$ ,  $R_t$  and  $W$ . Combined with the analysis of Table 2, it can be seen that the  $C_{dl}$  value increases by 9 times at 7 h-20 h. This shows that the double layer capacitance increases considerably. Because the determining factor of the electric double layer capacitance is the area where the charged ions are in contact with the metal surface, it can be concluded that the coating has been peeled off during the 7 h-20 h process. The  $R_t$  value in this period also increases by approximately 11 times. This increase indicates that the charge transfer inhibition caused by the filler such as filler in the coating becomes large. From 27 h to 48 h, the  $R_t$  value has tripled. This increase indicates that the barriers in the coating produce a superposition effect and the coating disbonding increases. After 27 hours, the  $R_t$  value fluctuates and eventually decreases. This decrease indicates that the coating disbonding enters another new stage and the degree of disbonding is large. This change can be confirmed again by the change in the  $W$  value, which represents a diffusion barrier to the mass transfer process. The value is first at a lower level and then exhibits a downward trend, which indicates that the coating is smoothly stripped.

**Table 3.** The impedance value of the components of the analog circuit of the test with AC interference of 8 V

	7 h	20 h	27 h	34 h	44 h	48 h
$C_c$	1.147E-7	1.385E-7	1.34E-7	1.683E-7	1.596E-7	1.743E-7
$R_c$	2.221	2.129	2.081	1.955	2.471	2.729
$C_{dl}$	0.1809	/	/	/	/	/
$R_t$	1.728	12.43	1.16	5.602	7.375	0.6985
$W$	/	0.3445	0.516	0.1703	0.1478	0.1531

In the tests with 8 V or 16 V AC interference, the best equivalent circuit for the spectrum at 7 h is C(R(RC)), and for the impedance spectrum measured after 7 h, the corresponding optimal equivalent circuit model is C(R(RW)).

**Table 4.** The impedance value of the components of the analog circuit of the test with AC interference of 16 V

	7 h	20 h	27 h	34 h	44 h	48 h
$C_c$	8.484E-8	6.53E-8	7.324E-8	7.952E-8	6.694E-8	6.622E-8
$R_c$	2.506	3.208	2.482	2.843	3.13	2.372
$C_{dl}$	0.001766	/	/	/	/	/
$R_t$	1.206	2.418	3.659	2.413	1.258	1.916
W	/	0.08364	0.08672	0.1571	0.2272	0.5659

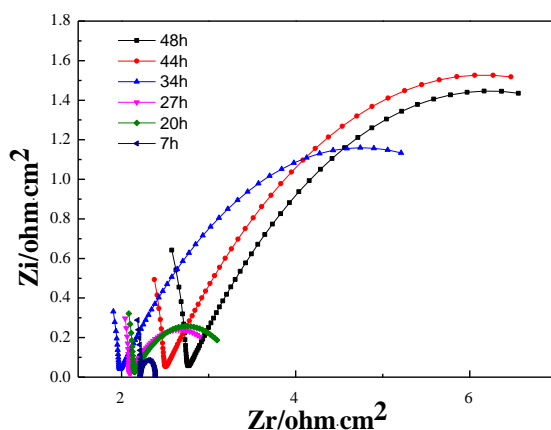


**Figure 10.** Nyquist diagrams of the test with AC interference of 8 V

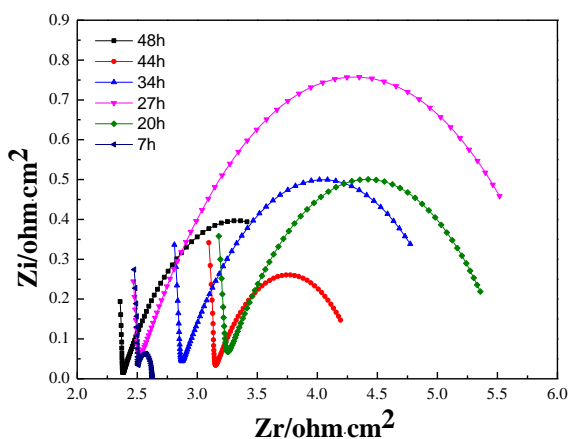


**Figure 11.** Nyquist diagrams of the test with AC interference of 16 V

The evolution of the impedance spectrum over time in the test system under 8 V AC interference is shown in Figure 10. The high-frequency arc range is within three, while the mid-low

frequency arc radius is much larger than that under 2 V or 4 V AC interference. After 34 h, the arc radius of the high frequency band clearly shifts to the right, that is, the radius of the arc ( $R_c$  value) shown in Table 3 becomes larger. Because the disbonding range and the gap increase, this creates more conditions for crevice corrosion (anode corrosion), and the cathode current shielding effect is intensified [38, 39]. Moreover, the AC interference of 8 V promotes the anodic corrosion, and thus, the impedance value caused by the corrosion product becomes larger, which is greater than the impedance reduction value caused by the disbonding of the coating, and the difference between the two is increased. Therefore, the  $R_c$  value increases after 34 h. At 20 h, the circuit model corresponding to the impedance spectrum has already appeared W impedance. This finding indicates that the promotion effect of 8 V AC interference on the cathode stripping of the coating is greater than that of 4 V or 2 V AC interference. The  $R_t$  value greatly increases correspondingly at 20 h. As shown in Figure 10, the arc radius of the middle and low frequency bands both increase with time, which is the superposition effect of the obstacles in the coating. The  $R_t$  value is almost 10 times the value interference with 4 V AC at 7 h, which shows that the degree of disbonding is greater than that in the 4 V AC test. In Table 3, the W value is reduced to a lower value, tends to be flat over time and is smaller than the W value in Table 2, which indicates that the disbonding of the coating continues to increase and the speed of corrosion increases.

The evolution of the impedance spectrum over time in the test system under 16 V AC interference is shown in Figure 11. The overall impedance range is smaller than that under AC 8 V interference, but there is the same movement phenomenon as that under AC 8 V interference. The arc radius of the low frequency band after 7 h is relatively large. As shown in Table 4, the  $R_c$  value interference with 16 V is the largest at 7 h AC in the four groups (2 V, 4 V, 8 V, 16 V AC) of experiments. This finding indicates that the AC of 16 V promotes the anodic corrosion most noticeably. The W value interference with 16 V AC appears at 20 h as the same as that interference with 8 V AC, which indicates that the coating has entered the stripping stage. The  $R_t$  value in the AC 16 V test at this time is larger than the  $R_t$  value at 20 h in the AC 8 V test, which indicates that the barrier effect of the coating in the AC 16 V test is greater during the solution diffusion process; that is, the degree of disbonding is greater. From 27 h to 44 h, the decrease in  $R_t$  value indicates that the coating disbonding has reached a stage where the solution diffuses to the internal gap of the coating, accompanied by a large area of cathodic disbondment. At 48 h, the  $R_t$  value increases, and the W value becomes larger, which indicates that a new stripping phase begins again. The mass transfer process encounters obstacles that need to be overcome, and the solution needs to refill these channels.

### 3.3. Effect on the disbonding distance of FBE anti-corrosion layer

**Table 5.** FBE anti-corrosion layer disbonding distance

AC voltage/V	0	2	4	8	16
Disbonding distance/mm	4.5	5.6	6.1	6.7	8.2



**Figure 12.** Physical diagram of AC interference disbonding test piece

As shown in Figure 12, under the interference of AC stray current, the disbonding distance of FBE anti-corrosion coating increases with the increase of interference intensity. This dynamic is consistent with the results exhibited by the cathodic protection current and electrochemical impedance spectroscopy.

### 3.4. Corrosion morphology analysis

Photographs were taken of the working electrode working faces at the end of the test period, after the working electrode working faces were cleaned and magnified 400 times with an SEM electron microscope, as shown in Figure 13 and Figure 14.

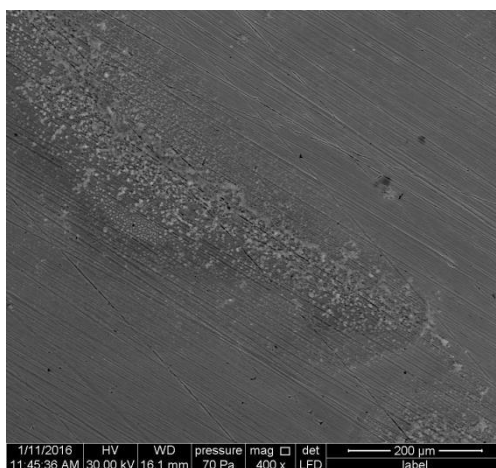


**Figure 13.** Microscopic morphology of metal surface without AC interference test

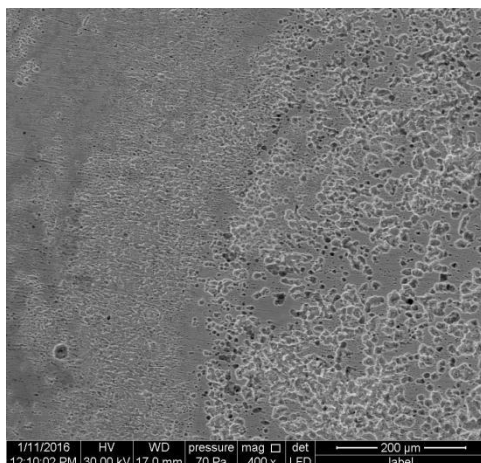


**Figure 14.** Microscopic morphology of metal surface in AC 8 V test

As shown in Figure 13, the microscopic topography of metal surface with noninterference test has only a small area of dull area and a small number of pits. As shown in Figure 14, the test piece was subjected to a combination of AC stray current and crevice corrosion to produce a plurality of closely arranged and concentrated corrosion concave surfaces, which are subjected to more severe corrosion.

The comprehensive microscopic morphology can confirm the reaction process of anodic corrosion in cathodic stripping. Moreover, since the cathodic stripping is accompanied by the cathode hydrogen evolution reaction and the crevice corrosion, the degree of anodic corrosion is aggravated by the interference of the alternating stray current, which indirectly causes the two reaction transition periods to be shortened and the stripping speed to be accelerated. That is, the stray current promotes the cathodic disbondment of the coating.

The composition of the exfoliated product analysis and its proportion is shown in Figure 15A, and the corresponding product analysis area is in the red square in Figure 15B.

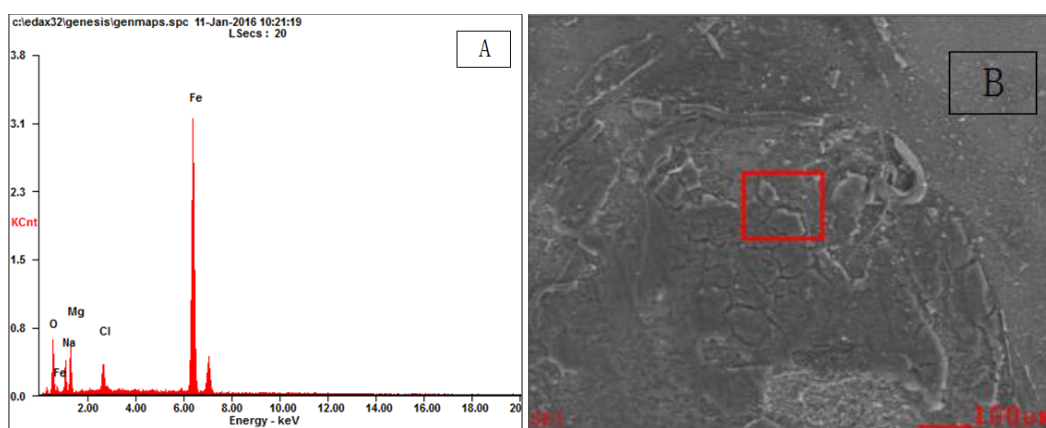


**Figure 15.** Product analysis diagrams (A:EDS; B:SEM)

As seen from Figure 15, the specific gravity of Fe is the largest, followed by O. This indicates that the disbonding product is mainly an oxide of Fe in the disbonding gap. In addition, the Na, Mg and Cl elements also have a certain proportion, and it is inferred that these three elements are mainly derived from the NaCl solution. In summary, the cathode stripping products that are not interfered by the coating are mainly oxides of Fe and crystals of NaCl and MgCl<sub>2</sub>.

#### 4. CONCLUSION

The effect on cathodic disbondment of the FBE anti-corrosion layer interaction with AC stray current was studied. By measurement and analysis of the cathodic protection current, electrochemical impedance spectroscopy and disbonding distance, the following rules were found:

(1) The AC stray current promotes the cathodic disbondment of the FBE coating, and under the same AC stray current intensity, the degree of disbonding of the coating increases with time. In the same test cycle, the greater the strength of the AC stray current applied to the test piece, the easier the FBE coating peeled off and the greater the degree of disbonding.

(2) At the critical disbonding of the coating and the metal surface, that is, the disbonding tip of the coating, whether it is macroscopic or microscopic, there is corrosion. This finding proves that the coating in the stripping process mainly occurs due to a cathodic hydrogen evolution reaction and anode crevice corrosion, and the two reactions are dominant at the same time. The applied AC stray current interference increases the rate of replacement of the hydrogen evolution reaction and the anodic corrosion on the coating strip. The greater the AC stray current is, the greater the disbonding of the coating.

#### ACKNOWLEDGMENTS

The research work was supported by Civil Aviation Safety Capacity Building Fund (Construction of safety evaluation system for multibranch complex annular apron pipe network) and Airport engineering research base open fund (Study on the optimization of cathodic protection model in the apron area based on BEASY).

#### CONFLICT OF INTERESTS

“The authors declare that there is no conflict of interests regarding the publication of this article.”

#### References

1. N. Parhizkar, T. Shahrabi, B. Ramezanzadeh. *J. Alloys Compd.*, 747 (2018) 109-123.
2. J. M. Yeh, H.Y. Huang, C. L. Chen, W. F. Su, Y. H. Yu, *Surf. Coat. Technol.*, 200 (8) (2006)2753-2763.
3. M. Sharifi, M. Ebrahimi, S. Jafarifard, *Prog. Org.Coat.*, 106 (2017) 69-76.
4. M.R. Bagherzadeh, T. Mousavinejad, *Prog. Org.Coat.*, 7 4 (3) (2012) 589-595.
5. G. Grundmeier, W. Schmidt, M. Stratmann, *Electrochim. Acta*, 45 (15) (2000) 2515-2533.
6. A. Ghanbari, M. Attar, *Surf. Coating. Technol.*, 246 (2014) 26-33.
7. S. Shreepathi, *Prog. Org.Coating*, 90 (2016) 438-447.

8. M. Mahdavian, R. Naderi, *J. Ind. Eng. Chem.*, 21 (2015) 1167-1173.
9. R. Naderi, M. Attar, *Prog. Org. Coating.*, 77 (2014) 830-835.
10. H. Bi, J. Sykes, *Prog. Org. Coating.*, 87 (2015) 83-87.
11. M.A. Alam, E.S.M. Sherif, S.M. Al-Zahrani, *Int. J. Electrochem. Sci.*, 8 (2013) 3121-3131.
12. E. Koehler, *Corrosion (Houston, TX, U. S.)*, 40 (1984) 5-8.
13. I. Ismail, M. K. Harun, *Rubber. Chem. Technol.*, 89(2012)712-723
14. H. Leidheiser Jr., *Corrosion*, 38 (1982)374.
15. M. Haji-Ghassemi, R.A. Cottis, K.R. Gowers, J.D. Scantlebury, *J. Oil Colour Chem. Assoc.*, 75 (1992) 277.
16. E.L. Koehler, *Corrosion*, 33 (1977) 209.
17. J.J. Ritter, *J. Coat. Technol.*, 54 (1982) 51.
18. N.W. Khun, G.S. Frankel, *Corros. Sci.*, 67 (2013) 152.
19. Y.L.Chen, W.Zhang, Q.Wang, J.Wang, *J Chin Soc Corr Pro.*, 37, 6(2017) 479-486.
20. P.A. Sørensen, C.E. Weinell, K. Dam-Johansen, S. Kiil *J. Coat. Technol. Res.*, 7(2010)773-786.
21. H. Leidheiser Jr., W. Wang, L. Igetoft, *Prog. Org. Coat.*, 11(1983) 19-40.
22. H. Leidheiser Jr., W. Wang, *J. Coat. Technol.* 53 (1981) 77.
23. S.B.Lyon, R.Bingham, D.J.Mills, *Prog.Org. Coat.*, 102(2017) 2-7.
24. S.Touzain, T.Q. Le,G.Bonnet,*Prog.Org. Coat.*, 52 (2005) 311.
25. Subrahmanya Shreepathi, *Prog. Org. Coat.*, 90 (2016) 438-447.
26. C.F. Dong, A.Q. Fu, X.G. Li, Y.F. Cheng, *Electrochim. Acta*, 54 (2008) 628-633.
27. X.Chen, X.G. Li, C.W. Du, Y.F. Cheng, *Corros. Sci.*, 51 (2009) 2242-2245.
28. J.J.Perdomo, I. Song, *Corros. Sci.*, 42 (2000) 1389-1415.
29. F.M. Song, N. Sridhar, *Corros. Sci.*, 50 (2008) 70-83.
30. E.O. Eltai, J.D. Scantlebury, E.V. Koroleva, *Prog. Org. Coat.*, 73 (2012) 8-13.
31. H.Bi ,J.Sykes,*Prog. Org. Coat.*, 87 (2015) 83-87.
32. A.Q. Fu, Y.F. Cheng, *Corros. Sci.*, 51 (2009) 914-920
33. D. Kuang and Y. F. Cheng, *Corros. Eng., Sci. Technol.*, 50 (2015) 211-217.
34. Jankowski. J. *Electrochem. So.*, 150 4(2003) B181-B191.
35. L.Y. Xu, X. Su, Y.F. Cheng, *Corros. Sci.*, 28 (2013) 263-268.
36. A. Junker, L. J. Belmonte, N. Kioupis, L. V.Nielsen, *Mater. Corros.*, 69 (9)(2018) 1170-1179.
37. Miwa. T, Takeshita. Y, Ishii. A, Sawada . T, *Prog.Org. Coat.*, 120(2018) 71-78.
38. Q. Liu,W. Wu,Y. Pan,Z.Y.Liu, *Constr. Build. Mater.*, 171,20(2018) 622-633.
39. X.H. Wang,Q. Liu,Y.C. Chun,Y.C. Li,Z.Q. Wang, *J. Mater. Eng. Perform.*, 27(2018) 3060-3071